# Generation and Evaluation of Hydrogelfacilitated 3D Tumor Microenvironments of Breast Cancer

Sheba Goklany<sup>1, #</sup>, Earl Brown<sup>2</sup>, Lauryn De La Torre<sup>1</sup>, & Kaushal Rege<sup>1,3 #</sup>

- <sup>1</sup> Chemical Engineering, School for Engineering of Matter, Transport, and Energy, Arizona State University, Tempe, AZ, 85287, USA.
- <sup>2</sup> Biomedical Engineering, School of Biological Health Systems Engineering, Arizona State University, Tempe, AZ, 85287, USA.
- <sup>3</sup> Biological Design, School for Engineering of Matter, Transport, and Energy, Arizona State University, Tempe, AZ, 85287, USA.

# # Corresponding authors:

Sheba Goklany
Chemical Engineering
501 E. Tyler Mall, ECG 303
Arizona State University
Tempe, AZ 85287-6106, USA
Email: <a href="mailto:sheba.goklany@asu.edu">sheba.goklany@asu.edu</a>

Kaushal Rege Chemical Engineering 501 E. Tyler Mall, ECG 303 Arizona State University Tempe, AZ 85287-6106, USA Email: rege@asu.edu

# **ABSTRACT**

Engineered three-dimensional (3D) cell culture models can accelerate drug discovery, and lead to new fundamental insights in cell-cell, cell-extracellular matrix, and cellbiomolecule interactions. Existing hydrogel or scaffold-based approaches for generating 3D tumor models do not possess significant tunability and possess limited scalability for high throughput drug screening. We have developed a new library of hydrogels, called Amikagels, which are derived from the crosslinking of amikacin hydrate and poly(ethylene alycol) diglycidyl ether (PEGDE). Here we describe the use of Amikagels for generating 3D tumor microenvironments (3DTMs) of breast cancer cells. Biological characteristics of these breast cancer 3DTMs, such as drug resistance and hypoxia were evaluated and compared to those of 2D monolayer cultures. Estrogen receptor (ER) positive breast cancer 3DTMs formed on Amikagels were more dormant compared to their respective 2D monolayer cultures. Relative to their respective 2D cultures, breast cancer 3DTMs were resistant to cell death induced by mitoxantrone and doxorubicin, which are commonly used chemotherapeutic drugs in cancer, including breast cancer. The drug resistance seen in 3DTMs was correlated with hypoxia seen in these cultures but not in 2D monolayer cultures. Inhibition of Mucin 1 (MUC1), which is overexpressed in response to hypoxia, resulted in nearly complete cell death of 2D monolayer and 3DTMs of breast cancer. Combination of an ER stress inducer and MUC1 inhibition further enhanced cell death in 2D monolayer and 3DTMs. Taken together, this study shows that the Amikagel platform represents a novel technology for the generation of physiologically relevant 3D tumor microenvironments in vitro and can serve as a platform to discover novel treatments for drug-resistant breast cancer.

### INTRODUCTION

Cell-based assays used for cancer drug discovery predominantly employ two dimensional (2D) monolayer cell cultures (1); however, 2D cultures do not adequately represent the physiological environment in vivo. Although 2D monolayer cultures are simple and still commonly used systems, these are not physiologically relevant because they do not mimic cell-cell interactions or the surrounding tumor microenvironment (2-4). Typically, 2D cultures do not recapture growth patterns, cell polarization and differentiation, expression of signaling molecules, and metabolism-associated proteins seen in tumor cells in vivo (5, 6). The mechanical and biochemical interaction between tumor cells and their microenvironment influences proliferation of cancer cells, inflammatory responses, as well as tumor vasculature (7); these cannot be captured in 2D monolayer cultures. Approximately 30% genes are differentially expressed in 2D cell cultures compared to tissues (7); genes upregulated in 2D cell cultures included those involved in cell cycling, metabolism, and macromolecule turnover whereas those downregulated in 2D cultures included genes involved in cell adhesion, cell-cell interaction with extracellular matrix (ECM), and membrane-associated signaling (7). Cellular phenotypic heterogeneity within the tumor is also marked by the presence of cancer stem cells (CSCs), a subset of malignant cells that are linked to drug resistance, tumor-initiation, self-renewal, and metastasis (8-10), but current in vitro models do not adequately recapitulate the interplay between tumor microenvironment and architecture on CSC content (8).

Mimicking the tissue microenvironment in vitro is indeed challenging because of the heterogeneity in cell types and numbers, cell-cell, cell-extracellular matrix, and cell-biomolecule interactions, protein and nucleic acid expression, and physiological conditions such as temperature, O<sub>2</sub> and CO<sub>2</sub> concentrations, and pH (11-13). However, considering costs associated with live animal studies, particularly for parallel drug screening, three dimensional (3D) in vitro models that are biologically relevant, reproducible, amenable to high throughput screening, and economical are urgently required to bridge the gap between laboratory and clinical testing (2). More representative 3D tumor microenvironments that recapitulate in vivo conditions including cell-cell and cell-matrix interactions, transport properties, hypoxia, nutrient deprivation, and drug

resistance, make these systems more relevant for studying gene and protein expression profiles compared to 2D monolayer models (14-17).

Different methods have been investigated for the development of 3D cell culture models for application in drug discovery, assay development, stem cell research, and implantation (1, 18-21). Scaffold-free techniques, including hanging drop, forced floating, and agitation-based methods do not require supports for the generation of 3D spheroids (22, 23). Spheroids can be also generated using a scaffold or matrix including those derived from biologically derived materials such as BD Matrigel™ basement membrane, Cultrex basement membrane, and hyaluronic acid (HA) or synthetic materials such as polyethylene glycol (PEG), polyvinyl alcohol (PVA), and poly(2-hydroxy ethyl methacrylate), and polylactide-co-glycolide (PLG) (1, 23). Some of the challenges associated with generating 3D tumor models for preclinical applications using these methods include generation of uniform, consistent, and reproducible spheroids, scalability to parallel screening / high-throughput platforms, tunability of the platform for multiple cell types, and / or the scale-up of drug screening for large libraries (24).

We have previously described the generation and characterization of aminoglycoside-derived hydrogels called Amikagels, which are generated by polymerization between amikacin hydrate and polyethylene glycol diglycidyl ether (PEGDE) or 1,4-butanediol diglycidyl ether (BDDE) (25-31). Amikagels facilitated the 3D culture of several cell types including 3D tumor microenvironments (3DTMs) of bladder cancer, that demonstrated cellular dormancy and resistance to anti-proliferative chemotherapeutic drugs (26) and stem cells for differentiation to islet-like cells (28). In this current study, we describe the use of Amikagels as a high-throughput platform for generating uniform and consistent 3D tumor microenvironments (3DTMs) of breast cancer cells. Breast cancer is the most common type of malignancy in women, accounting for 30% new cancer cases impacting more than 285,000 women every year within the United States. This disease is the second leading cause of cancer-related deaths in women, claiming over 43,000 lives each year (Cancer Facts and Figures 2022, American Cancer Society). Despite significant advances in detection techniques and chemo-, radio-, endocrine- and antibody-based

therapies, recurrence occurs in 20-40% of the patients as distant metastasis even decades after primary tumor diagnosis (32-34). The five-year survival rate for breast cancer that has spread to distant parts of the body is only 29% (American Cancer Society). In vitro models that closely resemble dormant and metastatic human breast cancer and their response to therapeutics are required identifying new effective therapeutics. The Amikagel platform provides a robust, versatile, economical, and high-throughput system for generating uniform 3D spheroids of different breast cancer cell lines. Our results indicate that breast cancer 3DTMs generated on Amikagels exhibited physiologically relevant characteristics in terms of hypoxia and drug resistance, and hence may be utilized for advancing novel therapeutic strategies for the treatment of breast cancer.

#### **EXPERIMENTAL**

Materials and methods.

Synthesis of Amikagels. Poly(ethylene glycol) diglycidyl ether (PEGDE,  $M_n$ = 500, Catalog # 475696) and amikacin hydrate (Catalog # A3650) were purchased from Sigma-Aldrich (St. Louis, MO). Ring-opening polymerization between amine groups in amikacin hydrate and epoxide group in PEGDE, in different stoichiometric ratios, was carried out as described previously for the synthesis of different Amikagel compositions (Table 1) (26, 28). Briefly, amikacin hydrate (0.171 moles) was dissolved in Nanopure® water (1 mL). The required volume of PEGDE was slowly added to the amikacin hydrate solution, resulting in a pre-gel which was filter-sterilized using a 0.2  $\mu$ m filter (Catalog # 431222). The filtrate (40  $\mu$ L) was pipetted into every well of a 96 well plate and the plate was incubated at 40°C for 7.5 h to enable gel formation. Sterile Nanopure® water (150  $\mu$ L) was added once to the Amikagels to remove any unreacted monomers and to keep the gels hydrated.

Cell culture. Human breast cancer cell lines, MDA-MB-231, MDA-MB-468, T47D, and MCF7, were cultured in DMEM (HyClone<sup>TM</sup> Dubelcco's Modified Eagles Medium) (GE Healthcare Life Sciences, Logan, Utah) supplemented with 10% fetal bovine serum (FBS, Atlanta Biologicals Inc., Lawrenceville, GA) and 1% penicillin/ streptomycin (10,000 units/mL; Sigma). Cells were maintained in an incubator at 37°C and 5% CO<sub>2</sub>. Cells were trypsinized at approximately 80% confluence with 1X trypsin (GE Healthcare Life Sciences) and seeded at a density of 50,000 cells/well suspended in 150 μL media in 96-well plates (Corning<sup>TM</sup> Costar<sup>TM</sup>, Corning, NY) for 2D monolayer culture studies, and allowed to attach overnight. 3DTMs of breast cancer were generated by plating 50,000 cells/well in 150 μL media on Amikagels in 96 well plates.

Flow cytometry for cell cycle analysis. Three 3DTMs for each cell line - MDA-MB-231, MDA-MB-468, T47D, and MCF7 - were collected in an Eppendorf tube; 50 μL of 5 mg/mL collagenase was added to the 3DTMs to facilitate their disassembly. The 3DTMs were disassembled by gentle pipetting and centrifuged at 1000 rcf to collect the cell pellet. The supernatant was discarded, and the cell pellet was washed twice with ice-cold 1X PBS. The cells were then resuspended in ice-cold 1X PBS solution of 1% (v/v) 1X Triton-X, 5% (v/v) fetal bovine serum (FBS), 50 μg/mL propidium iodide (PI) (ThermoFisher Scientific, Waltham, MA), and 0.006-0.01 units/mL of ribonuclease A (Sigma-Aldrich, St. Louis, MO). The cells were then incubated on ice for 30 minutes following which their cell cycle analysis was determined using flow cytometry. The PI signal was detected using an excitation of 535 nm and emission of 617 nm. For 2D monolayer cultures, cells were trypsinized, collected and processed similarly to the 3DTMs.

Drug treatments. T47D and MDA-MB-231 cells (50,000 cells/well) were seeded in cell culture treated 96 well plates for 2D monolayer or on Amikagels for 3DTM treatments overnight in DMEM media supplemented with 10% fetal bovine serum and 1% penicillin/streptomycin (10,000 units/mL). Mitoxantrone (topoisomerase II inhibitor) (Selleck Chemicals, Houston, TX), doxorubicin (topoisomerase II inhibitor) (Selleck Chemicals), HA15 (endoplasmic stress inducer) (Selleck Chemicals), and GO-203 (MUC1-C inhibitor)

(Selleck Chemicals) were dissolved in DMSO and added to the cells 24h following plating. The final DMSO (Thermo Fisher Scientific) concentration was maintained at 0.1% (v/v) in the well for all treatments. Cell viability was assessed 72 h following treatment with the drugs.

Cell viability measurements. 2D cell viability following drug treatment was determined using the 3-(4,5-Dimethylthiazol-2-yl)-2,5-diphenyltetrazolium bromide (Thermo Fisher Scientific) or MTT assay, a metabolic assay for proliferation, as described previously (35). T47D and MDA-MB-231 breast cancer cells (50,000 cells/well) were treated with mitoxantrone (topoisomerase II inhibitor; IC50 of 0.42 μM for MCF-7 cells), doxorubicin (inhibits topoisomerase II with an IC50 of 2.67 μM), HA15, or GO-203 at different dosages in 96 well plates. The MTT reagent (10 μL) was added to each well and incubated for 4 h at 37°C. The media was then aspirated and 50 μL of DMSO:methanol (Thermo Fisher Scientific) (1:1 v/v) was added to the wells. The plates were rotated at 37°C for 30 minutes. Sample absorbance was then determined at 570 and 670 nm using a plate reader (Bio-Tek Synergy 2), following which the cell viability was calculated (35). Briefly, the absorbance at 670 nm was subtracted from absorbance at 570 nm for a given sample and the data was normalized to the untreated sample. Cell viability for each treatment was reported as the average viability of three independent experiments; each individual experiment comprised three wells in triplicate.

Following drug treatments, cell viability of 3DTMs was determined using CellTiter-Glo® 3D Cell Viability Assay (Catalog # G9683, Promega, WI), specifically designed to determine viability in 3D spheroids, as per the manufacturer's protocol. The CellTiter-Glo® 3D Reagent results in cell lysis and a luminescent signal proportional to the amount of ATP present, which is proportional to the number of viable cells in culture (36). Briefly, 150  $\mu$ L CellTiter-Glo® 3D reagent was added to 150  $\mu$ L cell culture medium containing the 3DTM in each well in an opaque-walled 96 well plate. The contents were vigorously mixed for 5 minutes to induce cell lysis, following which, the plate was incubated for 25 minutes at room temperature. The luminescence was then recorded using a plate reader

(Bio-Tek Synergy 2) and viability was calculated by dividing the luminescence of the treated 3DTMs with that of the untreated 3DTMs (37, 38).

Drug penetration in 3DTMs. T47D cells (50,000 cells/well) were plated on AM5 Amikagels for 24h to enable 3DTM formation. At ~24 h, 3DTMs were treated with mitoxantrone (10  $\mu$ M) for 24h following which they were collected in Eppendorf tubes and fixed in 4% formaldehyde for 12 hours while being gently agitated on a rocker (Reliable Scientific, Hernando, MS). After 12 hours, the formaldehyde was gently removed, and the spheroids were washed with 1X PBS. Tissue Tek (VWR, Radnor, PA) was then added to the 3DTMs, which were then flash frozen and stored at -80°C prior to sectioning using a cryotome (Leica CM1950 Crystat) maintained at -17°C. Multiple spheroid sections (~ 40  $\mu$ m thickness) were cut and placed on a positively charged glass slide and dried at 37°C for 15 minutes and washed thrice with 1X PBS to remove the Tissue Tek. A drop of Fluoro-Gel with or without DAPI (Electron Microscopy Sciences, Catalog # 1798510 or 17985-50) was added to the sections prior to imaging using a Leica SP5 AOBS Spectral Confocal microscope.

Hypoxia Staining studies. 2D monolayer cultures and 3DTMs (50,000 cells/well) were treated with pimonidazole (100 μM, Hypoxyprobe<sup>TM</sup> Kit, Hydroyprobe, Inc., Burlington, MA), a 2-nitroimidazole-based surrogate marker for hypoxia, for 3 hours prior to fixation in 4% formaldehyde (*39*, *40*). Cells were then transferred into a 30% sucrose (Thermo Fisher Scientific) solution for 12 hours, frozen in Tissue Tek, and multiple spheroid sections (~ 40 μm thickness) were sectioned using a cryotome as described previously (*41*). Samples were permeabilized using a 0.1% Tween 20 (Thermo Fisher Scientific) solution in 1X phosphate buffer saline (PBS), blocked using a 10% Fetal Bovine Serum (FBS) (Thermo Fisher Scientific) solution in 1X PBS (*42*). Samples were then incubated with the primary antibody (1:50 dilution, Hypoxyprobe<sup>TM</sup> Kit, Hydroyprobe, Inc., Burlington, MA) overnight at 4°C followed by incubation with Goat Anti-Mouse IgG H&L (FITC) (1:1000, excitation: 493nm, emission: 528nm, ab6785, abcam, Cambridge, MA) for one hour at room temperature. Cells were counterstained with DAPI nuclear stain

(excitation: 358 nm, emission: 461 nm) and imaged using a Leica SP5 AOBS Spectral Confocal microscope (20X oil objective).

Statistical Analyses. All experiments were carried out at least in triplicate. All data were expressed as the mean ± standard error. One-way Analysis of Variance (ANOVA) was used to determine statistical significance, and p-values < 0.05 were considered statistically significant; The following convention was used to represent statistical significance ranges \*: 0.01<p-value<0.05 and \*\*: p-value<0.01.

#### **RESULTS AND DISCUSSION**

Amikagel synthesis and characterization for formation of breast cancer 3DTMs

Amikagels were formed by crosslinking the aminoglycoside amikacin hydrate (AH) with different molar ratios of polyethylene glycol diglycidyl ether (PEGDE) as described previously (26, 28). Different molar ratios of the monomers resulted in different compositions of Amikagels, AM3, AM4 and AM5 (Table 1), which, in turn, facilitated identification of the Amikagel formulation that results in breast cancer 3DTMs. Breast cancer cell lines, MDA-MB-231, MDA-MB-468, T47D, and MCF7, were plated on these different Amikagels in order to allow 3DTM formation by the liquid overlay method; MDA-MB-231, MDA-MB-468, and T47D 3DTMs formed the next day whereas MCF7 3DTMs formed after five days of plating; T47D 3DTMs did not form on AM3 and AM4 Amikagels, as indicated (in Figure 1). Only one 3DTM per well was observed, which indicated the high fidelity of this approach.

**Table 1.** Modulation of amikacin hydrate and PEGDE molar ratios for the synthesis of different Amikagels.

Amikacin hydrate (mole)	PEGDE (mole)	Molar ratio	Gel annotation
0.171	0.513	1:3	AM3
0.171	0.684	1:4	AM4
0.171	0.855	1:5	AM5

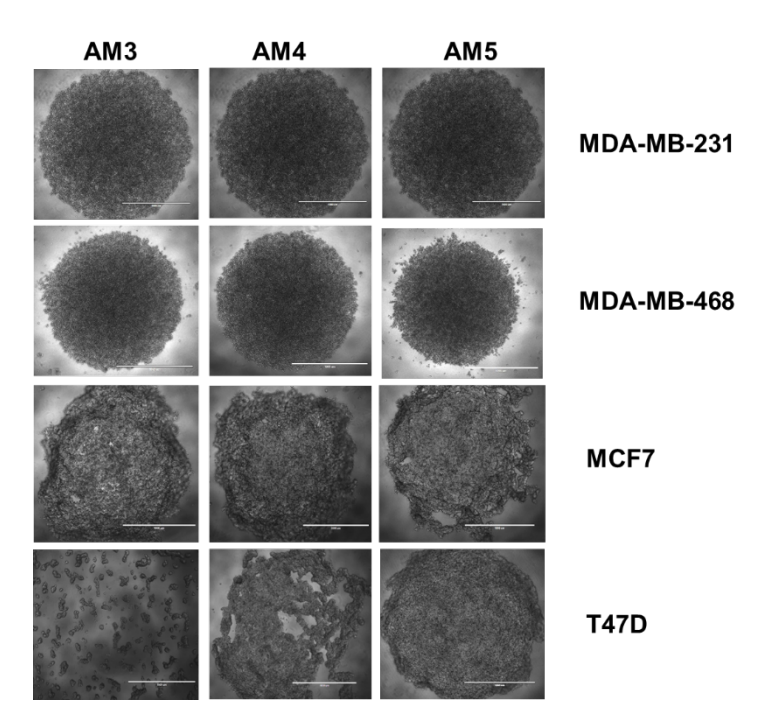


**Figure 1.** MDA-MB-231, MDA-MB-468, MCF7, and T47D 3DTMs plated on AM3, AM4, and AM5 Amikagels. T47D 3DTMs did not form on AM3 and AM4 Amikagels. Scale bar =  $1000 \mu m$ .

**Table 2.** Percentage cells in the G0/G1 phase of the cell cycle for MDA-MB-231, MDA-MB-468, MCF7, and T47D breast cancer cell lines on AM3, AM4, and AM5 Amikagels. Statistical significance was determined using one-way ANOVA and G0/G1 ratios on different Amikagels were compared to those for 2D cultures (\*\* indicates p < 0.01; n = 3 independent experiments).

Cell line	2D	AM3	AM4	AM5
MDA-MB-231	73 ± 3	77 ± 8	61 ± 4	63 ± 4
MDA-MB-468	68 ± 7	57 ± 7	56 ± 3	57 ± 5
MCF7	63 ± 2	81 ± 4 **	69 ± 5	60 ±4
T47D	66 ± 2	N/A	N/A	80 ± 5 **

Cell cycle arrest in the G0/G1 phase is a key characteristic of dormant tumor cells (26, 43), and the percentage of cells in the G0/G1 phase for 3DTMs was evaluated using flow cytometry (Table 2). 3DTMs of MCF7 and T47D cells, both estrogen receptor positive breast cancer cell lines, demonstrated a higher percentage of population in the G0/G1 phase of the cell cycle on AM3 and AM5 Amikagels, respectively, compared to 2D cultures, thereby indicating an increasing dormant-like phenotype under these conditions.

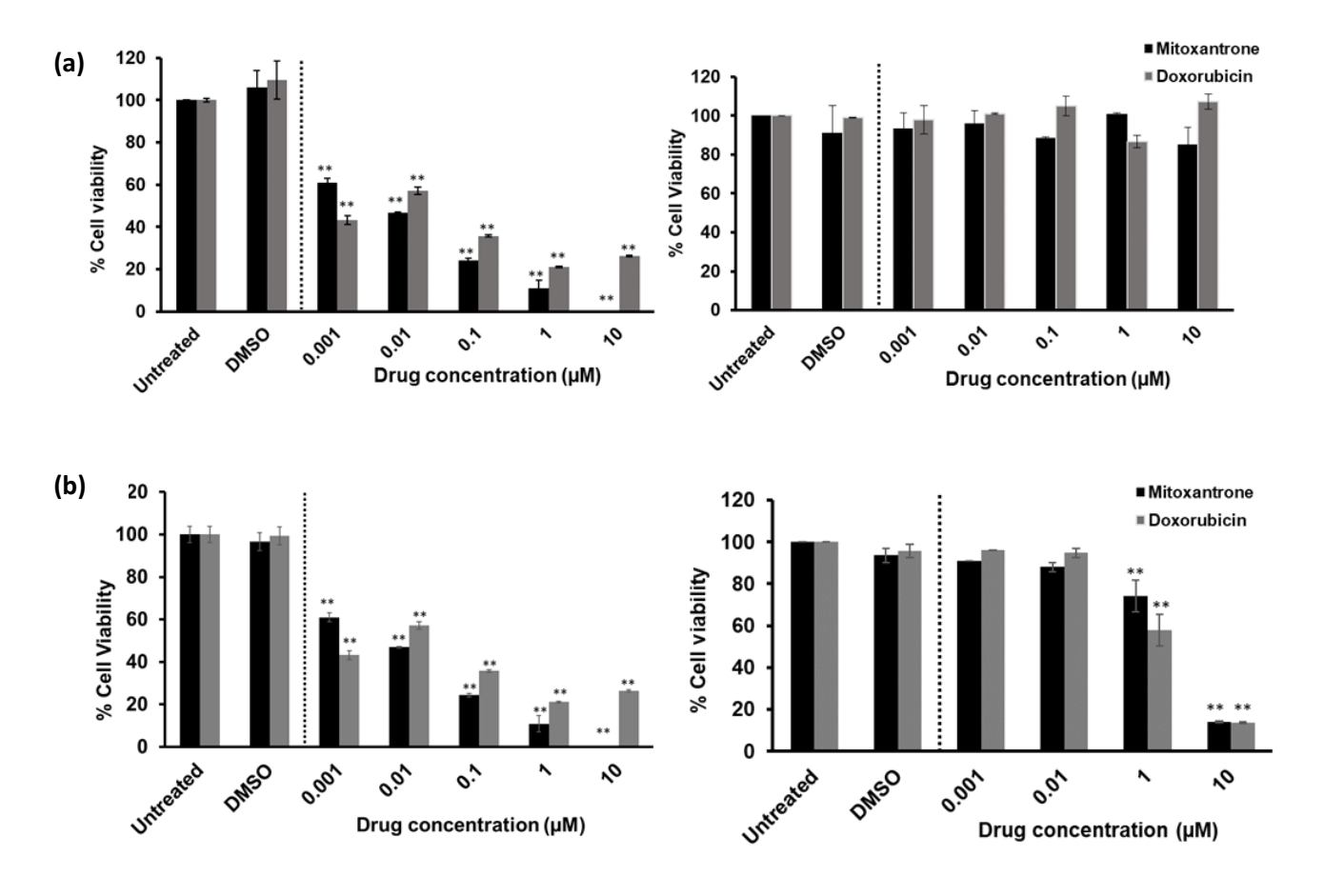


**Figure 2.** Cell viability (%) of 2D (left) and 3DTM (right) cultures of **(a)** T47D and **(b)** MDA-MB-231 breast cancer cells following treatment with different doses of mitoxantrone and doxorubicin for 72h. Statistical analysis was carried out by comparing mean cell viability values with untreated controls using one-way ANOVA (\*\* denotes  $p \le 0.01$ , n = 3).

MDA-MB-231 and T47D 3DTMs are more resistant to conventional DNA-damaging chemotherapeutic drugs than their respective 2D cultures.

Response of 3DTMs to chemotherapeutic drugs was evaluated using MDA-MB-231 and T47D cell lines, these represented proliferative and more dormant phenotypes on the Amikagels. MDA-MB-231 and T47D 3DTMs cultured on AM3 and AM5 Amikagels, respectively, were treated with different doses of mitoxantrone and doxorubicin. Mitoxantrone, as a single-agent or in combination with other chemotherapeutic drugs, has been used as a first-line treatment for advanced breast cancer (44-47). Doxorubicin hydrochloride and liposomal doxorubicin have also been FDA approved for the treatment

of breast cancer (*48*). 3DTMs greater than 500  $\mu$ m in diameter are better physiological representations of tumors compared to conventionally used 2D monolayer cultures since they recapture many cell-cell contact geometries, mass transfer limitations, and mechanical properties seen in vivo (*15*, *49*). T47D and MDA-MB-231 3DTMs, greater than 1000  $\mu$ m in diameter and treated with mitoxantrone (0.001 – 10  $\mu$ M) and doxorubicin (0.001 – 10  $\mu$ M) displayed greater drug resistance and higher cell viabilities compared to their respective 2D cultures (Figure 2). These reuslts are consistent with other reports in literature. For example, Melissaridou et al (2019) observed greater viability for 3D tumor spheroids of head and neck squamous cell carcinoma samples treated with cisplatin or cetuximab compared to 2D cultures (*50*). Imamura et al (2015) showed that BT-549, BT-474, and T47D breast cancer 3D multicellular spheroids were more resistant to paclitaxel and doxorubicin compared to 2D cultures (*51*). Indeed, we have shown that bladder cancer 3DTMs, generated on Amikagels, were resistant to conventional, DNA-damaging chemotherapeutics (*26*). T47D 3DTMs were chosen for subsequent analysis because of their greater drug resistance compared to that seen with MDA-MB-231 3DTMs.

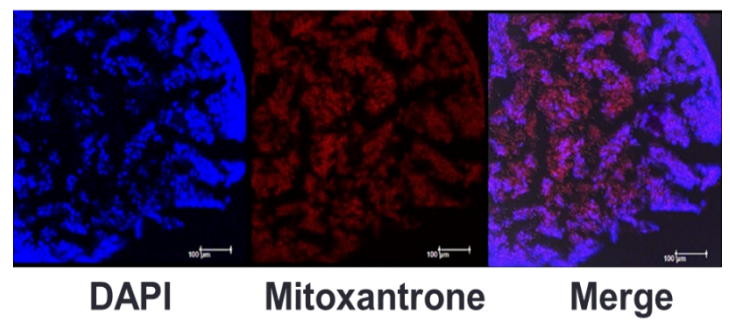


**Figure 3.** Drug penetration in T47D 3DTMs treated with 10  $\mu$ M mitoxantrone for 24h visualized by confocal fluorescence microscopy. Images from left to right indicate cell nuclei stained with DAPI (left panel; blue color; excitation: 350 nm, emission: 470 nm), mitoxantrone fluorescence emission signal in spheroids (center panel; red color; excitation: 610 nm; emission: 685 nm), and co-localization of mitoxantrone with DAPI (right panel). Figures are representation of sections taken from three different T47D 3DTMs from independent experiments (Scale bar = 100  $\mu$ m).

To evaluate whether administered drugs were able to penetrate 3DTMs, T47D 3DTMs were grown on AM5 Amikagels and treated with 10 µM mitoxantrone for 24h (52).

Mitoxantrone fluoresces with an excitation maxima at 610 and 660 nm, these signify the dimeric and monomeric forms of mitoxantrone, respectively (53), and an emission maximum at 685 nm (54); this signal was seen in the internal sections of the 3DTM (Figure 3, center panel, red color), and was observed to co-localize with cell nuclei, which were stained with DAPI (Figure 3, left panel). These results indicate that mitoxantrone penetrated the cell nuclei that that transport of the drug to the internal regions of 3DTMs was not limited.

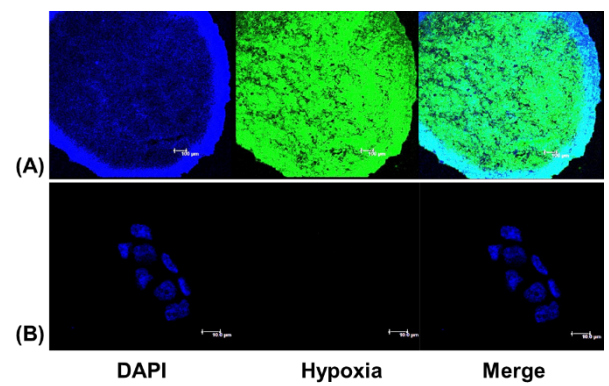


**Figure 4.** Hypoxia was observed in 3D T47D 3DTMs grown on AM5 Amikagels (A, center panel), but was not observed in 2D monolayer T47D cultures (B, center panel). Nuclei were stained with DAPI (left panel) and the merged image is depicted in the right-most panel. Images are representative of sections taken from three different T47D 3DTMs from independent experiments.

# Hypoxia in 3DTMs

Hypoxia, i.e., the state of reduced oxygen availability within tumors is considered to be a key driver of therapeutic resistance (49, 55). Cells in the external layer of solid human tumors have more access to oxygen compared to cells inside the tumor due to disorganized microcirculation, diffusion, and structural abnormalities within the tumor (49, 55). Hypoxia, mainly seen in the internal regions of tumors, can induce cellular quiescence, cell cycle arrest, differentiation, apoptosis, and necrosis in neoplastic tissue (55, 56). Multiple factors, such as inhibition of cell proliferation, hypoxia-induced reduced cytotoxic efficacy, and acidic tissue pH contribute to therapeutic resistance in hypoxic tumor tissue (57-61). In order to determine whether breast cancer 3DTMs grown on Amikagels exhibited hypoxia, T47D 3DTMs grown on AM5 Amikagels were evaluated for hypoxia 24h following plating using pimonidazole (40, 62). Our results showed that T47D 3DTMs grown on AM5 Amikagels exhibited hypoxia whereas 2D monolayer cultures of

T47D cells did not (Figure 4). It is likely that the hypoxia seen in T47D 3DTMs may, in part, be responsible for the cell cycle arrest and therapeutic resistance seen in these. Indeed, hypoxia has been shown to impart drug resistance and promote metastasis in breast cancer via the induction of hypoxia inducible factors (HIFs) that regulate several genes and proteins involved in tumor hypoxia and drug resistance (63-65).

Inhibition of MUC1 as a potential therapeutic target for hypoxic breast cancer tumors Mucin 1 (MUC1), a type I transmembrane protein, is expressed on the apical surface of mammary epithelial cells (66, 67). MUC1 acts as a transcriptional co-activator; its transmembrane subunit has a 72 residue-long cytoplasmic tail which contributes to its oncogenetic potential due to aberrant signaling interactions (67). MUC1 is aberrantly upregulated in tumors of epithelial origin, inhibits stress-induced apoptosis, and has been linked to tumor aggressiveness (66-70). Importantly, MUC1 has been shown to be overexpressed in hypoxic cells, leading to regulation of hypoxia-driven vascular endothelial growth factor-A and platelet-derived growth factor-B (71). Hypoxia is known to enhance MUC1 mRNA and protein expression via the transcriptional regulation of hypoxia-inducible transcription factor 1 or HIF-1α (72); Aubert et al (2009) showed that HIF-1α directly binds to the MUC1 promoter and enhances MUC1 expression under hypoxic conditions (73). HIF-1α modulates multiple cellular processes in tumor cells, including upregulation of drug efflux pumps that promote chemoresistance (67). MUC1, which is abundantly expressed in T47D cells, also enhances stability of HIF-1α (67, 74). MUC1 gene expression is upregulated by steroid hormones (66); the estrogen receptor alpha present in T47D cell lysate has been shown to regulate MUC1 expression by binding to MUC1 promoter estrogen receptor cis-elements (66). In order to further assess the consequences of hypoxia, we investigated the effect of GO-203, a MUC1 inhibitor, on 2D monolayer cultures and 3DTMs of T47D cells (Figure 5). Treatment with 100 μM and 200 μM GO-203 resulted in approximately 37% and 97% cell death in 3DTMs, respectively; cell death in 2D monolayer cultures at these GO-203 concentrations was greater than 95%. These results indicate that small-molecule inhibition of MUC1 can induce death of 3DTMs that demonstrate hypoxic behavior.

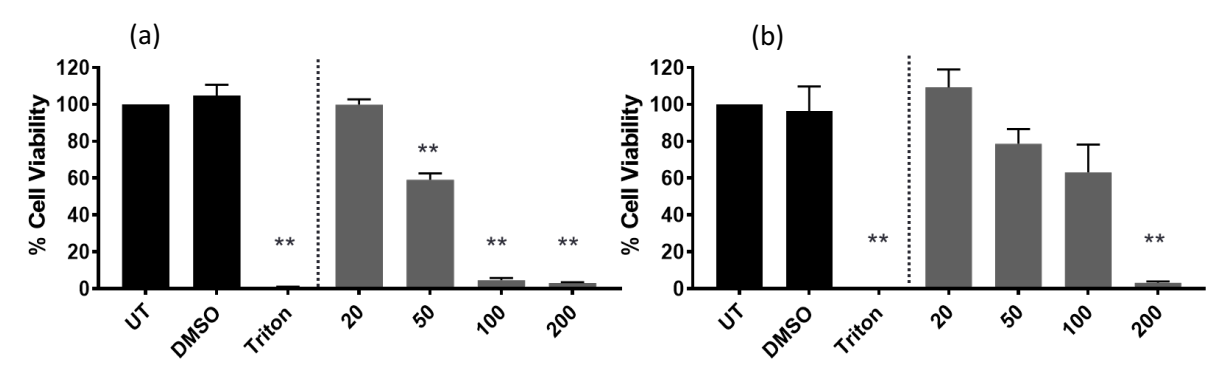


**Figure 5.** Cell viability (% of untreated or UT control) of (a) 2D monolayer T47D cultures and (b) T47D 3DTMs following treatment with different dosages of GO-203, a MUC1 inhibitor, for 72h. Statistical analysis was determined by using one-way ANOVA (\*\* denotes  $p \le 0.01$ , n = 3); all comparisons were made relative to the untreated control.

Endoplasmic reticulum (ER) stress activation for ablation of 3D breast cancer spheroids MUC1 expression is under the control of proteins involved in endoplasmic reticulum (ER) homeostasis (75); MUC1 is translated as a single polypeptide that undergoes autoproteolysis into two subunits in the endoplasmic reticulum (76-79). The MUC1 N-terminal subunit (MUC1-N) forms a stable complex with the C-terminal transmembrane subunit (MUC1-C) and is positioned extracellularly (76, 77). MUC1-N is released from the cell surface and MUC1-C is imported to the nucleus where it interacts with transcription factors involved in growth and survival as well as the mitochondrial outer membrane where it blocks apoptosis in response to stress (76, 77). Downregulation of MUC1 has been shown to enhance the unfolded protein response (UPR) signaling and cell death following ER stress. Tumor cells exhibit ER stress, thereby activating the unfolded protein response (UPR) which is characterized by attenuation of translation, upregulation of ER protein chaperones and foldases, ER-associated degradation to remove the irreparable misfolded proteins (75, 80, 81). The glucose-regulated protein 78 (GRP78) / immunoglobulin heavy chain-binding protein (BiP) is one the highest expressed ER resident chaperones and is a master regulator of the UPR (80). During ER homeostasis, GRP78 associates with three known UPR sensors: PKR-like ER kinase/pancreatic elF2a (eukaryotic translation initiation factor 2, a subunit) kinase (PERK/PEK), activating transcription factor 6 (ATF6), and inositol-requiring enzyme 1

(IRE1) (80, 82). Under conditions of ER stress, GRP78 dissociates from PERK, ATF6, and IRE1 to promote their signaling (80). Chronic or prolonged ER stress leads to cell death (80, 83). Studies have suggested that anterior gradient-2 (AGR2), an ER-localized chaperone involved in ER homeostasis, co-localizes with MUC1 and is essential for MUC1 expression (84). ARG2 is induced during ER stress via the activation of the ATF6 and IRE1 arms during UPR (85, 86). MUC1 knockdown cells showed enhanced UPR signaling and cell death following treatment with thapsigargin or glucose deprivation, both of which are ER stress inducers, compared to scrambled control cells treated with thapsigargin or glucose deprivation alone (75). Yin et al (2014) also showed that treatment of multiple myeloma cells with GO-203 and the proteome inhibitor bortezomib, an endoplasmic reticulum stress inducer, synergistically enhances reactive oxygen species and cell death (77). Previous work in our laboratory has shown that the combination of thapsigargin, an ER-specific calcium channel blocker, and bortezomib, a proteasome inhibitor, resulted in near complete ablation of bladder cancer 3DTMs, that were otherwise resistant to conventional chemotherapeutics including mitoxantrone (26). The combination treatment was seen to likely induce chronic ER stress leading to synergistic cell death compared to either treatment alone (26).

In this study, we evaluated the effect of HA15, a GRP78 inhibitor, as a single agent treatment and in combination with MUC-1 inhibition using 2D monolayer and 3DTMs of

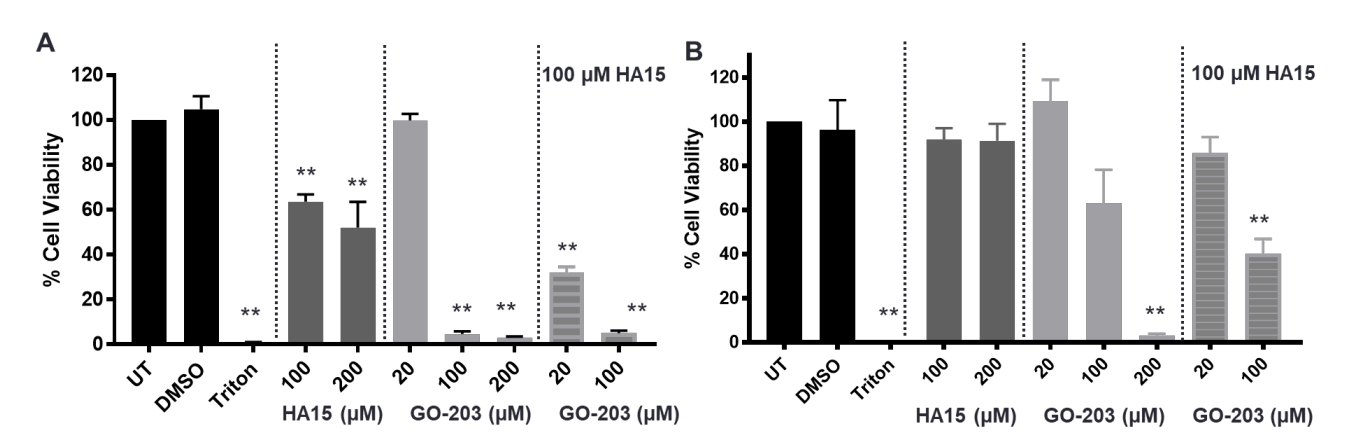


**Figure 6.** Cell viability (%) of (a) T47D 2D monolayer cultures, and (b) T47D 3DTMs following treatment with different doses of HA15, GO-203, and their combinations for 72h. Statistical significance was determined by using one-way ANOVA and all treatments were compared with respect to untreated (UT) controls (\*\* denotes  $p \le 0.01$ , n = 3).

T47D cells. HA15 is an ER stress inducer that specifically interacts with the GRP78 chaperone leading to cell death following induction of autophagy and apoptosis (87-89). In T47D 2D monolayer cultures, the combination of 100 μM HA15 and 20 μM GO-203, a MUC1 inhibitor, resulted in ~68% cell death, which was slightly elevated compared to individual treatments with 100 μM HA15 (cell death ~36%) and 20 μM GO-203 (no cell death, Figure 6a). In T47D 3DTMs, HA15 by itself did not cause any significant cell death (Figure 6b). However, treatment with the HA15 (100  $\mu$ M) and GO203 (20 or 100  $\mu$ M) combination led to a slight increase in cell death compared to GO203 alone in T47D 3DTMs (Figure 6b). For instance, treatment with 100 μM HA15 and 100 μM GO-203 resulted in approximately 8% and 37% cell death, respectively, whereas the combination led to 60% cell death (Figure 6b) in T47D 3DTMs. In 2D monolayer cultures, treatment with 100 µM and 200 µM HA15 resulted in approximately 36% and 48% cell death, respectively (Figure 6a). These results indicate that an ER stress inducer such as HA15 has the potential to ablate drug-resistant breast cancer and the combination of GO-203 and HA15 may represent a novel treatment for breast cancer, although detailed preclinical studies will have to be carried out to evaluate this further.

#### CONCLUSIONS

Relevant in vitro models that physiologically capture the tumor microenvironment are urgently needed to investigate treatment options for better clinical outcomes. Several 3D culture systems are cumbersome in operation and result in multiple spheroids of heterogeneous sizes (90-92). The aminoglycoside-derived Amikagel platform is a novel and powerful technology to generate 3D tissue microenvironments of different cell types (28, 93). This study successfully utilized the Amikagel platform to generate 3DTMs of different breast cancer cell lines. Formation of one viable 3DTM per well is a key advantage of using the Amikagel system because it can formation of uniform, reliable 3DTMs and enable economical, high-throughput drug screening for cancer and other diseases. The composition of Amikagels can be modulated to identify conditions that lead to the formation of breast cancer 3DTMs. Our results indicate that estrogen receptor positive cell lines displayed a modestly dormant phenotype on Amikagels compared to

their corresponding 2D monolayer cultures. 3DTMs generated on Amikagels were resistant to commonly used chemotherapeutic drugs, mitoxantrone and doxorubicin, and exhibited hypoxia. Knockdown of MUC1, a transmembrane protein expressed on the apical surface of mammary epithelial cells, enhanced cell death in 2D monolayer cultures and 3DTMs of breast cancer. We have also shown that the combination of GO-203, a MUC1 inhibitor, and HA15, a GRP78 inhibitor, potentially present a novel treatment for breast cancer. Taken together, the different characteristics of 3DTMs generated on the Amikagel platform should enable better predictions and outcomes for drug screens compared to 2D monolayer systems leading to acceleration of drug discovery. The Amikagel platform also has significant opportunities for improvement by incorporating different cell types and tumor vasculature, which will enable better simulation of physiological conditions in these in vitro models.

## **CONFLICTS OF INTEREST**

KR is affiliated with Synergyan, LLC.

### **ACKNOWLEDGEMENTS**

We are grateful to the Arizona Biomedical Research Center (ABRC; Grant ADHS16-162399 to SG) for funding this study; partial support from the NSF (Grant 170626 to KR) is also acknowledged. EB acknowledges support from the **KEEN** (https://entrepreneurship.engineering.asu.edu/asu-keen/) MORE and (https://graduate.engineering.asu.edu/more/) programs at ASU. We thank Dr. Sandra Gendler, David F. and Margaret T. Grohne Professor of Therapeutics in Cancer Research at the Mayo Clinic, Scottsdale, AZ for several helpful technical discussions on studies reported in this manuscript. We are also thankful to Dr. Karen Anderson, Professor at the Biodesign Center for Personalized Diagnostics at ASU, and Mr. Mark Knappenberger, Graduate Research Assistant at the Biodesign Center for Personalized Diagnostics at ASU, for help with the flow cytometer use.

#### REFERENCES

- 1. R. Edmondson, J. J. Broglie, A. F. Adcock, L. Yang, Three-dimensional cell culture systems and their applications in drug discovery and cell-based biosensors. *Assay and drug development technologies* **12**, 207-218 (2014).
- 2. M. Rimann, U. Graf-Hausner, Synthetic 3D multicellular systems for drug development. *Curr Opin Biotechnol* **23**, 803-809 (2012).
- 3. D. van den Brand, L. F. Massuger, R. Brock, W. P. R. Verdurmen, Mimicking Tumors: Toward More Predictive In Vitro Models for Peptide- and Protein-Conjugated Drugs. *Bioconjugate chemistry* **28**, 846-856 (2017).
- 4. M. F. Fisher, S. S. Rao, Three-dimensional culture models to study drug resistance in breast cancer. *Biotechnology and Bioengineering* **117**, 2262-2278 (2020).
- 5. K. Duval *et al.*, Modeling Physiological Events in 2D vs. 3D Cell Culture. *Physiology* (*Bethesda*, *Md.*) **32**, 266-277 (2017).
- 6. K. Chitcholtan, E. Asselin, S. Parent, P. H. Sykes, J. J. Evans, Differences in growth properties of endometrial cancer in three dimensional (3D) culture and 2D cell monolayer. *Exp Cell Res* **319**, 75-87 (2013).
- 7. A. Birgersdotter, R. Sandberg, I. Ernberg, Gene expression perturbation in vitro--a growing case for three-dimensional (3D) culture systems. *Semin Cancer Biol* **15**, 405-412 (2005).
- 8. D. S. Reynolds *et al.*, Breast Cancer Spheroids Reveal a Differential Cancer Stem Cell Response to Chemotherapeutic Treatment. *Scientific Reports* 7, 10382 (2017).
- 9. A. Singh, J. Settleman, EMT, cancer stem cells and drug resistance: an emerging axis of evil in the war on cancer. *Oncogene* **29**, 4741-4751 (2010).
- 10. H. Easwaran, H. C. Tsai, S. B. Baylin, Cancer epigenetics: tumor heterogeneity, plasticity of stem-like states, and drug resistance. *Mol Cell* **54**, 716-727 (2014).
- 11. G. Rijal, W. Li, Native-mimicking in vitro microenvironment: an elusive and seductive future for tumor modeling and tissue engineering. *J Biol Eng* **12**, 20 (2018).
- 12. M. Simian, M. J. Bissell, Organoids: A historical perspective of thinking in three dimensions. *The Journal of Cell Biology* **216**, 31-40 (2016).
- 13. A. P. Z. P. Fiore, P. d. F. Ribeiro, A. Bruni-Cardoso, Sleeping Beauty and the Microenvironment Enchantment: Microenvironmental Regulation of the Proliferation-Quiescence Decision in Normal Tissues and in Cancer Development. *Frontiers in Cell and Developmental Biology* **6**, 59 (2018).
- 14. F. Hirschhaeuser *et al.*, Multicellular tumor spheroids: an underestimated tool is catching up again. *J Biotechnol* **148**, 3-15 (2010).
- 15. G. Mehta, A. Y. Hsiao, M. Ingram, G. D. Luker, S. Takayama, Opportunities and challenges for use of tumor spheroids as models to test drug delivery and efficacy. *J Control Release* **164**, 192-204 (2012).
- 16. J. Friedrich, C. Seidel, R. Ebner, L. A. Kunz-Schughart, Spheroid-based drug screen: considerations and practical approach. *Nat Protoc* **4**, 309-324 (2009).
- 17. E. Fennema, N. Rivron, J. Rouwkema, C. van Blitterswijk, J. de Boer, Spheroid culture as a tool for creating 3D complex tissues. *Trends Biotechnol* **31**, 108-115 (2013).
- 18. V. M. Weaver *et al.*, Reversion of the malignant phenotype of human breast cells in three-dimensional culture and in vivo by integrin blocking antibodies. *J Cell Biol* **137**, 231-245 (1997).

- 19. K. Bhadriraju, C. S. Chen, Engineering cellular microenvironments to improve cell-based drug testing. *Drug Discov Today* **7**, 612-620 (2002).
- 20. H. Wang *et al.*, A novel model of human implantation: 3D endometrium-like culture system to study attachment of human trophoblast (Jar) cell spheroids. *Mol Hum Reprod* **18**, 33-43 (2012).
- 21. S. Breslin, L. O'Driscoll, Three-dimensional cell culture: the missing link in drug discovery. *Drug Discovery Today* **18**, 240-249 (2013).
- 22. R. Foty, A simple hanging drop cell culture protocol for generation of 3D spheroids. *Journal of visualized experiments : JoVE*, 2720 (2011).
- 23. R. L. F. Amaral, M. Miranda, P. D. Marcato, K. Swiech, Comparative Analysis of 3D Bladder Tumor Spheroids Obtained by Forced Floating and Hanging Drop Methods for Drug Screening. *Frontiers in Physiology* **8**, 605 (2017).
- 24. S. J. Han, S. Kwon, K. S. Kim, Challenges of applying multicellular tumor spheroids in preclinical phase. *Cancer Cell International* **21**, 152 (2021).
- 25. T. S. P. Grandhi *et al.*, Aminoglycoside Antibiotic-Derived Anion-Exchange Microbeads for Plasmid DNA Binding and in Situ DNA Capture. *ACS applied materials & interfaces* **6**, 18577-18589 (2014).
- 26. T. S. Pavan Grandhi, T. Potta, R. Nitiyanandan, I. Deshpande, K. Rege, Chemomechanically engineered 3D organotypic platforms of bladder cancer dormancy and reactivation. *Biomaterials* **142**, 171-185 (2017).
- 27. N. Raravikar *et al.*, Investigation into Pseudo-Capacitance Behavior of Glycoside-Containing Hydrogels. *ACS applied materials & interfaces* **9**, 3554-3561 (2017).
- 28. J. Candiello *et al.*, 3D heterogeneous islet organoid generation from human embryonic stem cells using a novel engineered hydrogel platform. *Biomaterials* **177**, 27-39 (2018).
- 29. K. N. Lin, T. S. P. Grandhi, S. Goklany, K. Rege, Chemotherapeutic Drug-Conjugated Microbeads Demonstrate Preferential Binding to Methylated Plasmid DNA. *Biotechnology Journal* **13**, 1700701 (2018).
- 30. I. Ridha, P. Gorenca, R. Urie, S. Shanbhag, K. Rege, Repulsion of Polar Gels From Water: Hydration-Triggered Actuation, Self-Folding, and 3D Fabrication. *Advanced Materials Interfaces* 7, 2000509 (2020).
- 31. A. Dobos, T. S. P. Grandhi, S. Godeshala, D. R. Meldrum, K. Rege, Parallel fabrication of macroporous scaffolds. *Biotechnol Bioeng* **115**, 1729-1742 (2018).
- 32. X. H. F. Zhang, M. Giuliano, M. V. Trivedi, R. Schiff, C. Kent Osborne, Metastasis Dormancy in Estrogen Receptor-Positive Breast Cancer. *Clinical cancer research: an official journal of the American Association for Cancer Research* 19, 10.1158/1078-0432.CCR-1113-0838 (2013).
- 33. H. Pan *et al.*, 20-Year Risks of Breast-Cancer Recurrence after Stopping Endocrine Therapy at 5 Years. *New England Journal of Medicine* **377**, 1836-1846 (2017).
- 34. J. Qin, J. Lian, S. Wu, Y. Wang, D. Shi, Recent Advances in Nanotechnology for Breast Cancer Therapy. *Nano LIFE* **09**, 1940003 (2019).
- 35. S. Goklany *et al.*, Delivery of TRAIL-expressing plasmid DNA to cancer cells in vitro and in vivo using aminoglycoside-derived polymers. *Journal of Materials Chemistry B* 7, 7014-7025 (2019).
- 36. S. P. M. Crouch, R. Kozlowski, K. J. Slater, J. Fletcher, The use of ATP bioluminescence as a measure of cell proliferation and cytotoxicity. *Journal of Immunological Methods* **160**, 81-88 (1993).

- 37. M. Zanoni *et al.*, 3D tumor spheroid models for in vitro therapeutic screening: a systematic approach to enhance the biological relevance of data obtained. *Scientific Reports* **6**, 19103 (2016).
- 38. Z. Zhang *et al.*, Establishment of patient-derived tumor spheroids for non-small cell lung cancer. *PLOS ONE* **13**, e0194016 (2018).
- 39. S. Riffle, R. N. Pandey, M. Albert, R. S. Hegde, Linking hypoxia, DNA damage and proliferation in multicellular tumor spheroids. *BMC cancer* 17, 338-338 (2017).
- 40. Y. Masaki *et al.*, Imaging Mass Spectrometry Revealed the Accumulation Characteristics of the 2-Nitroimidazole-Based Agent "Pimonidazole" in Hypoxia. *PLOS ONE* **11**, e0161639 (2016).
- 41. S. M. Hatfield *et al.*, Immunological mechanisms of the antitumor effects of supplemental oxygenation. *Science translational medicine* 7, 277ra230-277ra230 (2015).
- 42. A. A. Narkhede, J. H. Crenshaw, D. K. Crossman, L. A. Shevde, S. S. Rao, An in vitro hyaluronic acid hydrogel based platform to model dormancy in brain metastatic breast cancer cells. *Acta Biomaterialia* **107**, 65-77 (2020).
- 43. C. Prunier *et al.*, Breast cancer dormancy is associated with a 4NG1 state and not senescence. *npj Breast Cancer* 7, 140 (2021).
- 44. K. Landys, S. Borgstrom, T. Andersson, H. Noppa, Mitoxantrone as a first-line treatment of advanced breast cancer. *Invest New Drugs* **3**, 133-137 (1985).
- 45. W. R. Bezwoda, R. Dansey, L. Seymour, First-Line Chemotherapy of Advanced Breast Cancer with Mitoxantrone, Cyclophosphamide and Vincristine. *Oncology* **46**, 208-211 (1989).
- 46. T. D. Shenkenberg, D. D. Von Hoff, Mitoxantrone: a new anticancer drug with significant clinical activity. *Ann Intern Med* **105**, 67-81 (1986).
- 47. B. Lu, S.-B. Xiong, H. Yang, X.-D. Yin, R.-B. Chao, Solid lipid nanoparticles of mitoxantrone for local injection against breast cancer and its lymph node metastases. *European Journal of Pharmaceutical Sciences* **28**, 86-95 (2006).
- 48. J. Lao *et al.*, Liposomal Doxorubicin in the treatment of breast cancer patients: a review. *Journal of drug delivery* **2013**, 456409-456409 (2013).
- 49. A. S. Nunes, A. S. Barros, E. C. Costa, A. F. Moreira, I. J. Correia, 3D tumor spheroids as in vitro models to mimic in vivo human solid tumors resistance to therapeutic drugs. *Biotechnology and Bioengineering* **116**, 206-226 (2019).
- 50. S. Melissaridou *et al.*, The effect of 2D and 3D cell cultures on treatment response, EMT profile and stem cell features in head and neck cancer. *Cancer cell international* **19**, 16-16 (2019).
- 51. Y. Imamura *et al.*, Comparison of 2D- and 3D-culture models as drug-testing platforms in breast cancer. *Oncol Rep* **33**, 1837-1843 (2015).
- 52. H. Gaskell *et al.*, Characterization of a Functional C3A Liver Spheroid Model. *Toxicol. Res.* **5**, (2016).
- 53. M. Enache, E. Volanschi, Spectral characterization of self-association of antitumor drug mitoxantrone. *Revue Roumaine de Chimie* **55**, (2010).
- 54. D. H. Bell, Characterization of the fluorescence of the antitumor agent, mitoxantrone. *Biochim Biophys Acta* **949**, 132-137 (1988).
- 55. M. Höckel, P. Vaupel, Tumor Hypoxia: Definitions and Current Clinical, Biologic, and Molecular Aspects. *JNCI: Journal of the National Cancer Institute* **93**, 266-276 (2001).

- 56. E. O. Pettersen, T. Lindmo, Inhibition of cell-cycle progression by acute treatment with various degrees of hypoxia: modifications induced by low concentrations of misonidazole present during hypoxia. *British journal of cancer* **48**, 809-817 (1983).
- 57. B. A. Teicher, J. S. Lazo, A. C. Sartorelli, Classification of antineoplastic agents by their selective toxicities toward oxygenated and hypoxic tumor cells. *Cancer Res* **41**, 73-81 (1981).
- 58. J. S. Bedford, J. B. Mitchell, The effect of hypoxia on the growth and radiation response of mammalian cells in culture. *The British Journal of Radiology* **47**, 687-696 (1974).
- 59. J. L. Wike-Hooley, J. Haveman, H. S. Reinhold, The relevance of tumour pH to the treatment of malignant disease. *Radiother Oncol* **2**, 343-366 (1984).
- 60. N. Raghunand, R. J. Gillies, pH and drug resistance in tumors. *Drug Resist Updat* **3**, 39-47 (2000).
- 61. J. W. Wojtkowiak, D. Verduzco, K. J. Schramm, R. J. Gillies, Drug resistance and cellular adaptation to tumor acidic pH microenvironment. *Molecular pharmaceutics* **8**, 2032-2038 (2011).
- 62. C. Azuma, J. A. Raleigh, D. E. Thrall, Longevity of Pimonidazole Adducts in Spontaneous Canine Tumors as an Estimate of Hypoxic Cell Lifetime. *Radiation Research* **148**, 35-42 (1997).
- 63. C. E. McAleese, C. Choudhury, N. J. Butcher, R. F. Minchin, Hypoxia-mediated drug resistance in breast cancers. *Cancer Lett* **502**, 189-199 (2021).
- 64. D. Generali *et al.*, Phosphorylated ERalpha, HIF-1alpha, and MAPK signaling as predictors of primary endocrine treatment response and resistance in patients with breast cancer. *J Clin Oncol* **27**, 227-234 (2009).
- 65. E. Favaro, S. Lord, A. L. Harris, F. M. Buffa, Gene expression and hypoxia in breast cancer. *Genome Medicine* **3**, 55 (2011).
- 66. J. Z. Zaretsky *et al.*, MUC1 gene overexpressed in breast cancer: structure and transcriptional activity of the MUC1 promoter and role of estrogen receptor alpha (ERα) in regulation of the MUC1 gene expression. *Molecular Cancer* **5**, 57 (2006).
- 67. K. Mehla, P. K. Singh, MUC1: a novel metabolic master regulator. *Biochim Biophys Acta* **1845**, 126-135 (2014).
- 68. M. D. Walsh, S. M. Luckie, M. C. Cummings, T. M. Antalis, M. A. McGuckin, Heterogeneity of MUC1 expression by human breast carcinoma cell lines in vivo and in vitro. *Breast Cancer Res Treat* **58**, 255-266 (1999).
- 69. N. Agata *et al.*, MUC1 oncoprotein blocks death receptor-mediated apoptosis by inhibiting recruitment of caspase-8. *Cancer research* **68**, 6136-6144 (2008).
- 70. I. S. Reynolds *et al.*, Mucin glycoproteins block apoptosis; promote invasion, proliferation, and migration; and cause chemoresistance through diverse pathways in epithelial cancers. *Cancer and Metastasis Reviews* **38**, 237-257 (2019).
- 71. S. Kitamoto *et al.*, MUC1 enhances hypoxia-driven angiogenesis through the regulation of multiple proangiogenic factors. *Oncogene* **32**, 4614-4621 (2013).
- 72. Y. Mikami, A. Hisatsune, T. Tashiro, Y. Isohama, H. Katsuki, Hypoxia enhances MUC1 expression in a lung adenocarcinoma cell line. *Biochemical and Biophysical Research Communications* **379**, 1060-1065 (2009).
- 73. S. Aubert *et al.*, MUC1, a New Hypoxia Inducible Factor Target Gene, Is an Actor in Clear Renal Cell Carcinoma Tumor Progression. *Cancer Research* **69**, 5707 (2009).

- 74. M. D. Walsh, S. M. Luckie, M. C. Cummings, T. M. Antalis, M. A. McGuckin, Heterogeneity of MUC1 expression by human breast carcinoma cell lines in vivo and in vitro. *Breast Cancer Research and Treatment* **58**, 253-264 (1999).
- 75. A. A. Olou, R. J. King, F. Yu, P. K. Singh, MUC1 oncoprotein mitigates ER stress via CDA-mediated reprogramming of pyrimidine metabolism. *Oncogene* **39**, 3381-3395 (2020).
- 76. D. W. Kufe, Mucins in cancer: function, prognosis and therapy. *Nature Reviews Cancer* **9**, 874-885 (2009).
- 77. L. Yin, T. Kufe, D. Avigan, D. Kufe, Targeting MUC1-C is synergistic with bortezomib in downregulating TIGAR and inducing ROS-mediated myeloma cell death. *Blood* **123**, 2997-3006 (2014).
- 78. F. Levitin *et al.*, The MUC1 SEA module is a self-cleaving domain. *J Biol Chem* **280**, 33374-33386 (2005).
- 79. B. Macao, D. G. Johansson, G. C. Hansson, T. Härd, Autoproteolysis coupled to protein folding in the SEA domain of the membrane-bound MUC1 mucin. *Nat Struct Mol Biol* **13**, 71-76 (2006).
- 80. J. Wu, R. J. Kaufman, From acute ER stress to physiological roles of the Unfolded Protein Response. *Cell Death Differ* **13**, 374-384 (2006).
- 81. M. Song *et al.*, IRE1α–XBP1 controls T cell function in ovarian cancer by regulating mitochondrial activity. *Nature* **562**, 423-428 (2018).
- 82. I. Kim, W. Xu, J. C. Reed, Cell death and endoplasmic reticulum stress: disease relevance and therapeutic opportunities. *Nat Rev Drug Discov* 7, 1013-1030 (2008).
- 83. R. Sano, J. C. Reed, ER stress-induced cell death mechanisms. *Biochim Biophys Acta* **1833**, 3460-3470 (2013).
- 84. A. M. Norris *et al.*, AGR2 is a SMAD4-suppressible gene that modulates MUC1 levels and promotes the initiation and progression of pancreatic intraepithelial neoplasia. *Oncogene* **32**, 3867-3876 (2013).
- 85. L. Dumartin *et al.*, ER stress protein AGR2 precedes and is involved in the regulation of pancreatic cancer initiation. *Oncogene* **36**, 3094-3103 (2017).
- 86. E. Chevet *et al.*, Emerging roles for the pro-oncogenic anterior gradient-2 in cancer development. *Oncogene* **32**, 2499-2509 (2013).
- 87. M. Cerezo *et al.*, Compounds Triggering ER Stress Exert Anti-Melanoma Effects and Overcome BRAF Inhibitor Resistance. *Cancer Cell* **29**, 805-819 (2016).
- 88. D. Xu *et al.*, Endoplasmic Reticulum Stress Signaling as a Therapeutic Target in Malignant Pleural Mesothelioma. *Cancers* **11**, 1502 (2019).
- 89. C. Ruggiero *et al.*, The GRP78/BiP inhibitor HA15 synergizes with mitotane action against adrenocortical carcinoma cells through convergent activation of ER stress pathways. *Mol Cell Endocrinol* **474**, 57-64 (2018).
- 90. J. P. Celli *et al.*, An imaging-based platform for high-content, quantitative evaluation of therapeutic response in 3D tumour models. *Sci. Rep.* **4**, (2014).
- 91. S. Chandrasekaran, Y. Geng, L. A. DeLouise, M. R. King, Effect of homotypic and heterotypic interaction in 3D on the E-selectin mediated adhesive properties of breast cancer cell lines. *Biomaterials* **33**, 9037-9048 (2012).
- 92. R.-Z. Lin, L.-F. Chou, C.-C. Chien, H.-Y. Chang, Dynamic analysis of hepatoma spheroid formation: roles of E-cadherin and β1-integrin. *Cell Tissue Res* **324**, 411-422 (2006).

93. B. Miryala, Z. Zhen, T. Potta, C. M. Breneman, K. Rege, Parallel Synthesis and Quantitative Structure-Activity Relationship (QSAR) Modeling of Aminoglycoside-derived Lipopolymers for Transgene Expression. *ACS Biomaterials Science & Engineering*, (2015).